Orbital
The electronic journal of chemistry

the electronic journal of chemistry

Full Paper | http://dx.doi.org/10.17807/orbital.v14i1.1642

Bilastine Based Drugs as SARS-CoV-2 Protease Inhibitors: Molecular Docking, Dynamics, and ADMET Related Studies

Ajoy Kumer [a, b*], Unesco Chakma [c], and Mohammed M. Matin* [d]

Bilastine drugs, structurally piperidine-1-carboxylate and sulfonyloxyethyl carboxylate derivatives, have significantly been employed as the medication of second-generation antihistamine drugs, and are used for the treatment of allergic rhinoconjunctivities and urticarial (hives). The bilastine drugs, composed of benzene carboxylate, propanoate, carboxylate, methyl-sulfonate, propanoic acid, butanoic acid, and pentanoic acid derivatives, were investigated through computational tools against SARS-CoV-2. The COVID-19 virus consists of five proteases where the curial function is performed by main proteases (M^{pro}) and Spike proteases (S^{pro}). The M^{pro} and S^{pro} were selected for calculation of molecular docking by these bilastine drugs which showed higher binding energy (<-6.5 kcal/mol) for both proteases. The main carboxylic acid group in bilastine drugs is found the primary key for a high binding score to show the large binding affinity with M^{pro} and S^{pro}, and is highly responsible for forming the hydrogen bond although the various hydrophobic bonds were produced as a weak interaction. For justification, the stability of molecular docked ligand-protein complexes was investigated with molecular dynamics. It showed that the root mean square deviation (RMSD) and root mean square fluctuation (RMSF) of all these drugs were below the 0.9 Å after residue interaction. Moreover, the HOMO-LUMO gap, hardness, and softness provided full details for their chemical reactivity. In this view, the pharmacokinetics and Lipinski rule were calculated, and all of these molecules had satisfied the Lipinski rule. Finally, using the admetSAR online database, absorption, distribution, metabolism, excretion, and toxicity have been calculated which indicated that these bilastine drugs are non-carcinogenic and less harmful for both aquatic and non-aquatic species.

Graphical abstract

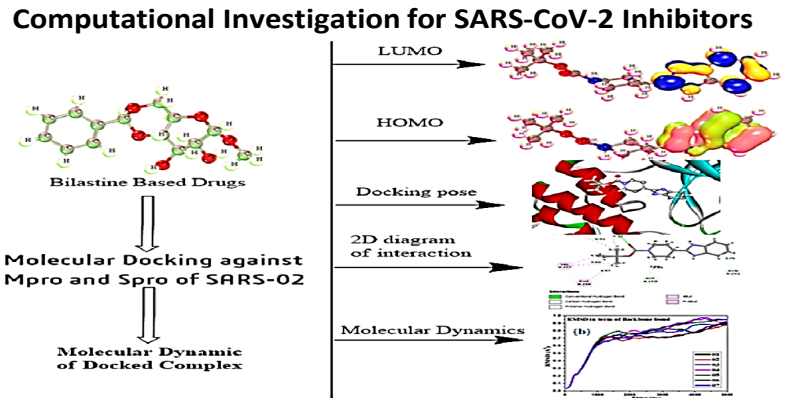

Keywords

Inhibition constant
Drug-likeness
Molecular docking
Molecular Dynamics
SARS-CoV-2

Article history

Received 09 June 2021
Revised 08 August 2021
Accepted 22 January 2022
Available online 23 March 2022

Handling Editor: Arlan Gonçalves

[a] Department of Chemistry, European University of Bangladesh, Gabtoli, Dhaka-1216, Bangladesh. [b] Department of Chemistry, Bangladesh University of Engineering and Technology, Dhaka, 1000, Bangladesh, [a] Department of Electrical and Electronics Engineering, European University of Bangladesh, Gabtoli, Dhaka-1216, Bangladesh, [d] Bioorganic and Medicinal Chemistry Laboratory, Department of Chemistry, University of Chittagong, Chittagong, 4331, Bangladesh *Corresponding author. E-mail: **kumarajoy.cu@gmail.com** or **mahbubchem@cu.ac.bd**

1. Introduction

SARS-CoV-2 has been spreading all over the world as an invisible enemy and caused millions of people within a couple of years. It was first introduced in Wuhan state of Republic China in November 2019, and our globalization has disconnected from one community to another community where continued existence is the largest challenge for human beings. Some prominent scientists recommended it as a biological weapon for destroying human beings although the human beings previously won the challenge outbreaks pandemics, such as SARS-1, ZIKA virus, Soyan flu, Spanish flu, HIV, AIDS, third plague pandemic, Asian flu, Hong Kong flu, third cholera pandemic and bird flu with the blessings of science and technology. First of all, SARS-CoV-2 was identified as lethal endemic diseases, such as Extreme Acute Respiratory Syndrome (SARS) and endemic Middle East Respiratory Syndrome (MERS) which has been caused by a coronavirus. This virus consists of chemically a single-stranded with a positive-sense RNA genome, sub-family Coronavirinae in the family Coronaviridae and the order Nidovirales [1], and is almost similar to human beta-coronaviruses, such as SARS-CoV-1, and MERS-CoV, but also has a small variation in their genomic and phenotypic structure that can manipulate their pathogenesis [2]. It could be found after chemical analysis as a spherical or pleomorphic enveloped particle, club-shaped glycoprotein projections, RNA allied to a nucleoprotein within a capsid composed of matrix protein. In general, SARS-CoV-2 composes of at least six open reading frames, such as spike glycoprotein, envelope, small membrane protein, membrane protein, hemagglutinin-esterase, nucleoprotein, and genomic protein. Among them, the two crucial polypeptides, hymotrypsin-like protease (3CL^{pro}) or main protease (M^{pro}) and spike protease (S^{pro}), are responsible for their chemical change and physiological tasks. The biological structure of SARS-CoV-2 is composed of the membrane (M) glycoprotein, the outer surface or cover of the common side consisting of a short unique *N*-terminal fragment (-NH_2) connected with the spike protein (staying the most outside of the body as a hook, which can attach the host body), and a long -COOH terminus of the cytoplasmic domain is added with the virion (inside) [3].

There are many studies for developing new drugs and vaccines based on the main protease (M^{pro}) which is the RNA binding using the *N*-terminal domain (NTD) of nucleocapsid protein (N protein) [4]. Although the completely alleviated drugs and vaccines were not invented for treatment, the computational study has been making the scope of quick and low-cost research on drug discovery About a couple of years back, there were some studies about drug discovery as inhibitors of SARS-CoV-2 by antivirus drugs [5], proteinase and 2-*O*-ribose methyltransferase [6], chymotrypsin-like protease inhibitors [7], protein ion channel [8], Moroccan medicinal plants [9], guanosine derivatives [10], potential multi-target-directed ligands based drugs [11], Andrographolide as a potential inhibitor [12], natural products [13], stilbene-based natural compounds [14], different Saikosaponins [15] and *Moides verticillata* components harvested from Western Algeria [16]. Moreover, vaccination was also predicted using computational tools by angiotensin-converting enzyme-2 and furin (protease enzyme) [17].

There has not been any prescribed drug for the treatment of SARS-CoV-2 by the world health organization, till now so far, and do not know exactly what will happen in the near future by this pandemic. But, it is true without the prescription of WHO that some countries have been benefiting from the use of chloroquine, hydroquinone, chloroquine phosphate, etc. [18] although there is no evidence, so far, a hundred percent cure of the disease. However, some traditional drugs were simulated based on computational tools in our work, which are commercially named bilastine group drugs, and are the derivatives of piperidine-1-carboxylate and sulfonyloxyethyl carboxylate. The main point is to select these drugs having a long -COOH terminus that can play a significant role in drug-protein interaction by evaluating the computational study. Moreover, the derivatives of piperidine-1-carboxylate were used as an antifungal drug, NR2B subtype-selective *N*-methyl-D-aspartate (NMDA) antagonists [19], AChE and BChE inhibitors [20], potent HIV-1 NNRTIs [21], dual inhibitory potency against acetylcholinesterase and Aβ1–42 aggregation for Alzheimer's disease therapeutics [22], and inhibitor of novel influenza virus [23]. Besides, these derivatives were also recognized as the potential drug for Type 2 diabetics [24], and VEGF receptor tyrosine of kinase inhibitors [25]. Regarding these potential applications in medical treatment, these were selected for the study of binding inhibitors against SARS-CoV-2 M^{pro} and S^{pro}. Molecular docking, initially introduced by Kuntz et al. 1982 [26], belongs to a computational method that virtually seeks to predict a complex of two binding partners, such as biological macromolecules and small molecules as drugs. Molecular dynamics and inhibition constant of the ligand-protein complex were calculated for their stability and drug potential activity.

2. Results and Discussion

2.1 Optimized structures of bilastines 1-7

Seven piperidine-1-carboxylate and benzenesulfonates (**1**-**7**) with different pharmacophore groups were simulated for geometry optimization by computational tools through the DFT method and the optimized chemical structures of these compounds are listed in **Fig. 1** with molecular name.

2.2 HOMO, LUMO, and chemical reactivity descriptors

The computed εLUMO, εHOMO and Δε gap, chemical potential (μ), electronegativity (χ), hardness (η), softness (S) and electrophilicity (ω) of drugs using the B3LYP functional of DFT method from DMol code of material studio are presented in Table 1. The εLUMO, and εHOMO magnitudes are useful tools for the evaluation of chemical reactivity and hydrophobic or electrophilic attraction with macromolecules [27-30]. Moreover, the HOMO-LUMO gap is directly related to the chemical stability of molecules [31-38], which is also predicted by the softness value or the hardness value. It was evident from Table 1 that compounds **6** and **7** showed the lowest softness value.

The frontier molecular orbital (FMO) has determined the chemical reactivity and active sites for binding with protein. The lower magnitude of the energy gap contributes to forming higher stability or the lower possibility of dissociation. The FMO of the compounds is presented in Fig. 2.

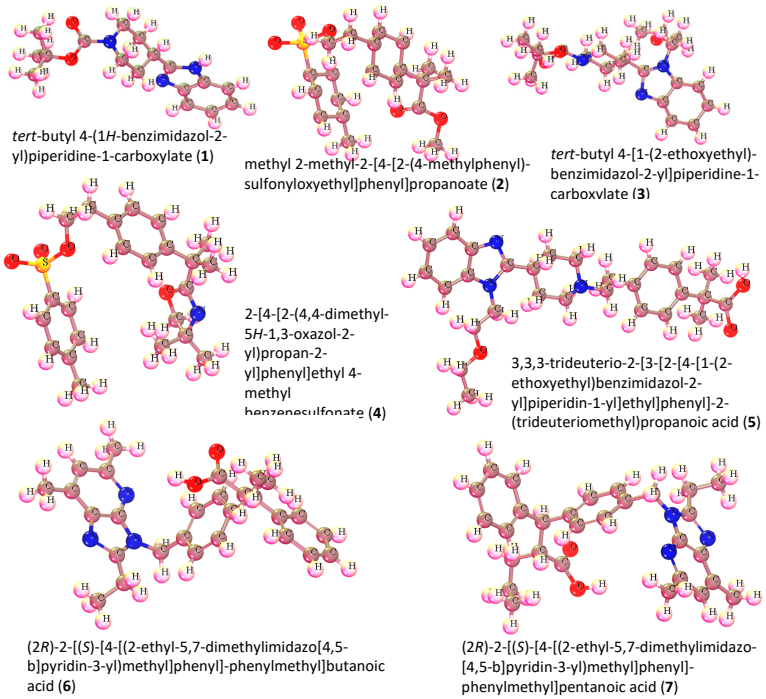

Fig. 1. Optimized structures of bilastine type compounds **1**-**7.**

Table 1. Frontier molecular orbitals and Reactivity descriptor analysis.

Drug	εLUMO, (eV)	εHOMO (eV)	εHOMO-εLUMO gap (eV)	Ionization potential (I), eV	Electron affinity (A), eV	Chemical potential (μ), eV	Hardness (η, eV)	Electrons activity (x, eV)	Electro-philicity (w, eV)	Softness (S, eV)
1	-0.350	-8.219	7.869	8.219	0.350	-4.284	3.934	4.284	2.333	0.254
2	-1.870	-8.866	6.996	8.866	1.870	-5.368	3.498	5.368	4.112	0.285
3	-0.207	-8.314	8.107	8.314	0.207	-4.260	4.053	4.260	2.238	0.246
4	-2.047	-8.679	6.632	8.679	2.047	-5.363	3.316	5.363	4.336	0.301
5	-0.405	-8.136	7.731	8.136	0.405	-4.270	3.865	4.270	2.358	0.258
6	-0.005	-8.913	8.908	8.913	0.005	-4.459	4.454	4.459	2.231	0.224
7	-0.088	-8.922	8.834	8.922	0.088	-4.505	4.417	4.505	2.297	0.226

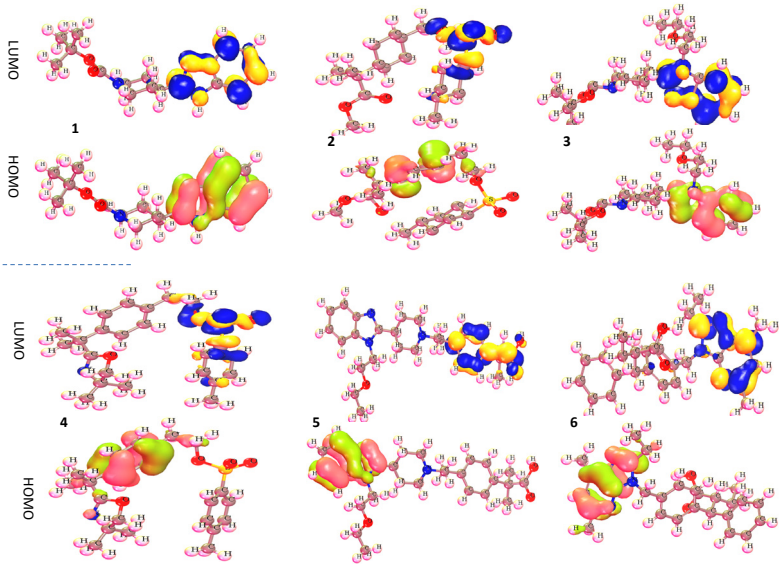

Fig. 2. Frontier molecular orbital (FMO) for HOMO and LUMO.

In the case of LUMO, the yellow color indicates the negative node and the blue color indicates the positive node of orbitals. On the other hand, the violet color for HOMO indicates the positive node of pink, and the light green color expresses the negative node of orbitals. It must be mentioned that the protein can be attached to the part of LUMO, which is

illustrated in the piperidine part of the compound containing the nitrogen atom. For both LUMO and HOMO, the carboxylate group has no contribution to electrophilic and nucleophilic attraction. However, the piperidine group is the most important part of bilastine group drugs for drug discovery.

2.3 Molecular docking study

Molecular docking studies were conducted with the ligand and protein interaction on the basis of various force field interactions calculated as binding affinity and are shown in Table 2. The binding affinity plays an important role for primary screening of ligand-protein interaction in view of observing the H bonding and hydrophobic bonding for docking score where the docking score from -5.50 kcal/mol to -7.7 kcal/mol (Table 2) had recorded which indicated as a standard drug for M^{pro} [39-40]. The study clearly indicated that carboxylate, propanoate, methyl benzenesulfonate, propanoic acid, butanoic acid, and pentanoic acid could be considered as the standard drug considering this standard docking score in terms of binding energy (Table 2).

Table 2. Data of binding energy and number of interacted bonds for M^{pro}.

Ligand/Drug	Binding Affinity (kcal/mol)	No. of H bond	No. of Hydrophobic bond	No. of van der Waal bond	Total bonds
1	-6.5	03	06	Absent	09
2	-5.5	04	03	Absent	07
3	-6.5	03	08	Absent	11
4	-6.6	04	03	Absent	07
5	-7.7	05	05	Absent	10
6	-7.4	03	03	Absent	05
7	-7.2	Absent	04	Absent	04

In the next stage, molecular docking was conducted with S^{pro}, which showed good binding energy toward the target protein ranging from -5.30 to -7.30 kcal/mol and presented in Table 3. The bilastine compounds **5**, **6**, and **7** showed binding energy -7.3, -7.6, and -7.0 kcal/mol, respectively. It could be said that compounds **5**, **6**, and **7** are highly active inhibitors against both S^{pro} and M^{pro}. Secondly, the activity of **5** and **6** has found the most activity among all drugs although they have superior potentiality against S^{pro} and M^{pro}. There are small changes in H bonding and hydrophobic bonding between S^{pro} and M^{pro} where more H bonding is observed for S^{pro}. In general, the molecular docking scores indicated that all these bilastine molecules (except **2**) possess a higher potentiality for inhibition against S^{pro} and M^{pro}.

Table 3. Data of binding energy and number of interacted bonds for S^{pro}.

Ligand/Drug	Binding Affinity (kcal/mol)	No. of H bond	No. of Hydrophobic bond	No. of van der Waal bond	Total bonds
1	-6.3	02	05	Absent	07
2	-5.3	Absent	03	Absent	03
3	-6.7	01	08	Absent	09
4	-6.5	02	01	Absent	03
5	-7.3	01	16	Absent	17
6	-7.6	03	06	Absent	09
7	-7.0	02	09	Absent	11

2.4 Calculation of inhibition constant for M^{pro} and S^{pro}

In the case of molecular docking, five other parameters, such as inhibition constant (Ki), intermolecular energy, electrostatic energy, torsion energy, unbounded energy of docked protein-ligand complex were also determined by auto dock tools. It should be noted that the Ki is directly proportional to binding energy, and theoretically, it is expressed as IC_{50}. The IC_{50} or inhibition constant demonstrated ranging from 12.23 to 70.51 μM for the M^{pro} (Table 4) and 18.05 to 373.49 μM for S^{pro} (Table 5) where the standard value of inhibition constant has been established in the 80.08 μM. Thus, from the inhibition constant for M^{pro}, it could be revealed that all selected molecules were better than any standard, but it could slightly depart from the standard value for S^{pro}. Moreover, the intermolecular energy is proportionally decreased with increasing the value of inhibition constant, and it was found ranging between -7.20 to -9.80 kcal/mol for M^{pro} and -4.45 to -7.46 kcal/mol for S^{pro}.

Table 4. Data of inhibition constant (Ki) for M^{pro}.

Drug (Ligand)	Inhibition constant (μM)	Ligand efficiency	Inter-molecular energy (kcal/mol)	Vdw-hb-desolv energy (kcal/mol)	Electrostatic energy (kcal/mol)	Torsional energy (kcal/mol)	Unbond energy (kcal/mol)
1	24.03	-0.29	-7.20	-7.13	-0.07	0.89	-0.47
2	23.68	-0.24	-8.70	-8.70	-0.13	2.39	-1.34
3	25.12	-0.23	-8.36	-8.24	-0.13	2.09	-1.45
4	13.69	-0.23	-8.72	-7.60	-1.12	2.09	-1.50
5	12.23	-0.20	-9.98	-9.23	-0.76	3.28	-1.45
6	39.24	-0.20	-8.80	-8.85	-0.56	2.49	-1.45
7	70.51	0.17	8.65	7.72	0.93	2.98	-1.55
7	363.85	-0.13	-7.42	-7.25	-0.16	2.98	-1.88

Table 5. Data of inhibition constant (Ki) for S^{pro}.

Drug (Ligand)	Inhibition constant (μM)	Ligand efficiency	Internal energy (kcal/mol)	Vdw-hb-desolv energy (kcal/mol)	Electrostatic energy (kcal/mol)	Torsional energy (kcal/mol)	Unbond energy (kcal/mol)
1	280.63	-0.22	-5.74	-5.74	-0.04	0.89	-0.05
2	373.49	-0.18	-7.06	-6.99	-0.07	2.39	-1.30
3	18.05	-0.09	-4.45	-4.45	-0.02	2.09	-1.54
4	253.18	-0.17	-6.99	-6.93	-0.06	2.09	-1.75
5	32.29	-0.06	-5.32	-4.32	-1.32	3.28	-2.19
6	318.08	-0.14	-7.46	-6.7	-1.39	2.68	-1.39
7	363.85	-0.13	-7.42	-7.25	-0.16	2.98	-1.88

2.5 Protein-ligand interactions

After molecular docking, binding interactions between the active sites of ligands and proteins were considered. Table S01 and Table S02 (supplementary file) indicated that proteins and ligands are linked by two types of bonds, such as H bonding interaction and hydrophobic bonds. The basic reason for the strong hydrogen bond effect is due to its shorter bond distance (~3.0 Å) which is less than other bond distances. On the other hand, some types of hydrophobic bonds have been formed which are considered to be weak bonds because their bond distance is between 4.0 and 5.0 Å. For each protein-ligand interaction, it is found that the number of hydrophobic bonds is two to three times greater than the number of hydrogen bonds, resulting in a binding affinity value. A close review of all the Tables S01 and S02 also reveals that the binding side changes with any change. No specific binding site was found in the same protein that could inactivate all of the drugs on the site. This means that, so far, no specific amino acids have been found inside ligands and proteins that are close to all molecules as normal sites.

2.6 Molecular dynamics (MD)

Molecular dynamics is an unrivaled method for determining the stability of any protein-ligand complex after docking, and the stability/existence of any protein-ligand complex can be determined from this study. Molecular dynamics is also used to diagnose various important factors [41] such as - how long a protein can be attached to its opposite/binder compound, how long it can be attached to any environment with protein, how changes can occur in that environment due to the effect of temperature, how to change their tendency to be attached to biological systems over longer-times. After simulating the molecular dynamics, it was informed about the RMSD and RMSF values in the protein-ligand complex. The universally accepted value of these two parameters is considered below 2.0 Å with any variable [42]. If more than that, then all these complexes lose their stability after entering the biological system, and it is considered as non-binder [43, 44]. After docking with the M^{pro}, molecular dynamics are generally taken in time and amino acid residue variable with RMSD and RMSF magnitude. The RMSD was found that when there was no interaction between them, their value was close to 2.4 Å (Fig. 3a) and it was slightly decreased after the formation of the hydrogen bond ranging about 2.1 Å (Fig. 3c). It can be said that hydrogen bonding is not sufficiently responsible for its stability. One of the reasons for this is that its value stands at around 0.8 Å as opposed to amino acids, which gives this complex the longest stability. It showed a similar trend for RMSF.

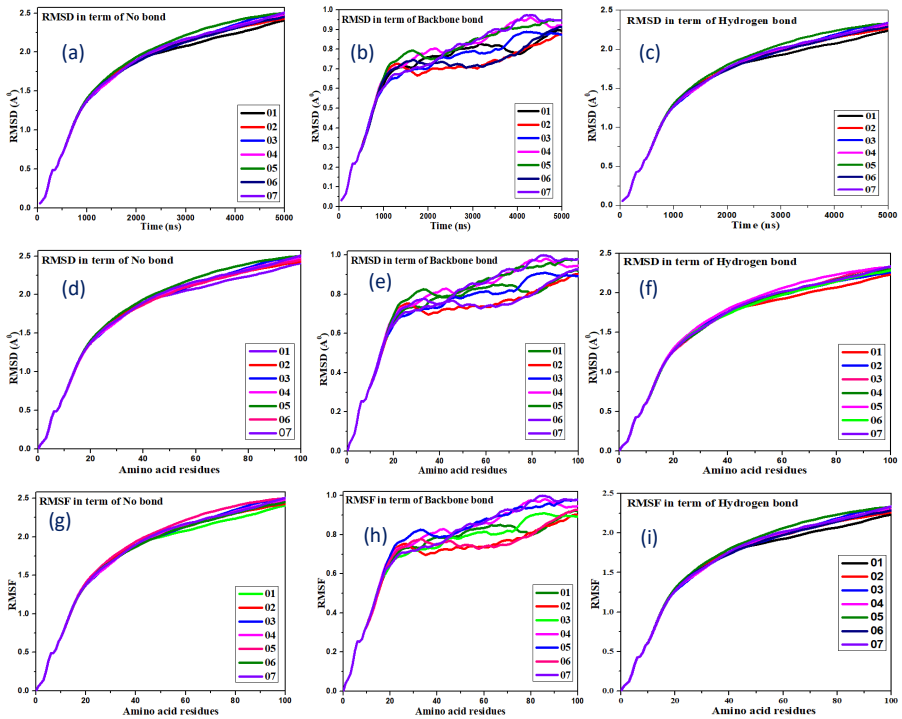

Fig. 3. Various graphs for main protein (M^{pro}) vs bilastines. RMSD: (a) Time vs no bond; (b) Time vs protein skeleton; (c) Time vs Hydrogen bond; (d) Amino acid vs no bond; (e) Amino acid vs backbond; (f) Amino acid vs H bond. RMSF: (g) Amino acid vs no bond; (h) Amino acid vs backbond; (i) Amino acid vs H bond.

In the case of Spro, the MD was performed on the basis of RMSD and RMSF for the protease and ligand-complex after docking (Fig. 4). The RMSD value is about 3.0 Å, which has occurred without any bond between protein and ligand interaction. It decreased by about 1.4 Å, which indicated the standard for drug discovery. When the H bond is created, the RMSD is about 2.9 Å while the RMSF was about 3.0 Å which is not a good result for standard drugs. However, when bonds were created as backbone bonds with protein residue, the RMSD was 1.6 to 1.0 Å and RMSF was about 1.6 to 1.2 Å for the first six drugs. In the case of H bonds, both of RMSD and RMSF were found about 3.0 Å (Fig. 4).

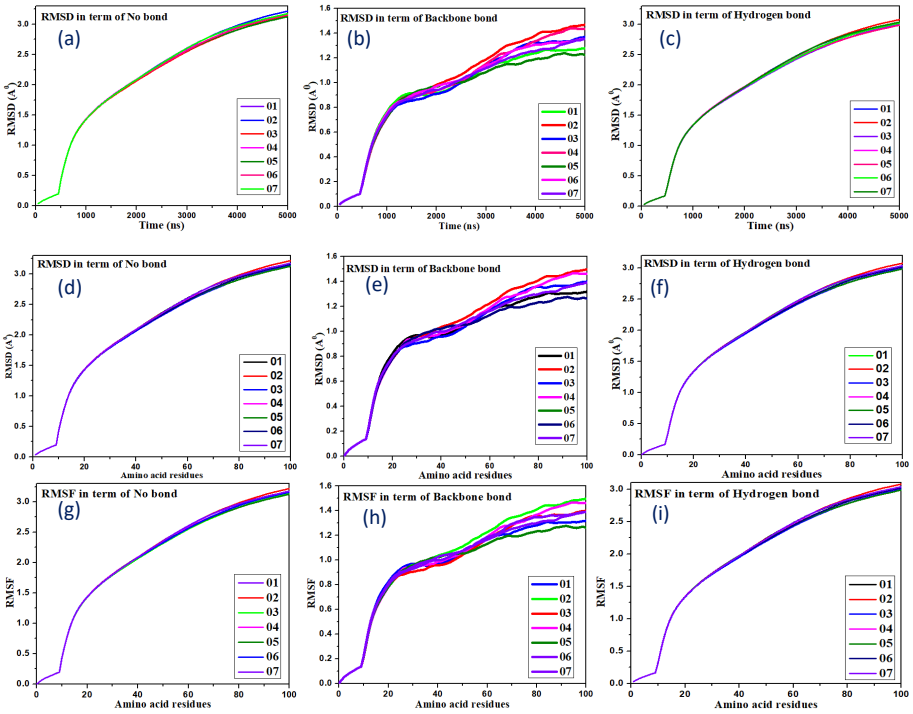

Fig. 4. Various graphs for main protein (Spro) vs bilastines. RMSD: (a) Time vs no bond; (b) Time vs protein skeleton; (c) Time vs Hydrogen bond; (d) Amino acid vs no bond; (e) Amino acid vs backbond; (f) Amino acid vs H bond. RMSF: (g) Amino acid vs no bond; (h) Amino acid vs backbond; (i) Amino acid vs H bond.

2.7 Pharmacokinetics and drug-likeness study

According to Christopher A. Lipinski's rule for drug molecules (1997) stated that first of all, it should have less than 5 hydrogen bond donors, less than 10 hydrogen bond acceptors, and the number of rotatable bonds should be three or more, but the molecular mass should be less than 500 Daltons [45]. The fifth view is the octanol-water partition coefficient expressed as log P0/w and it is not greater than 5.

The Swiss Institute of Bioinformatics online database was used to evaluate the Pharmacokinetics and drug-likeness applying the Lipinski rule from the log in the mentioned link https://www.sib.swiss/, and make a comparison study as drug activity [46, 37]. As shown in Table 6, all the molecules are found to follow the Lipinski rule as a potential drug(s). Although all molecules are established and approved drugs, the unveiling of their Lipinski Rules has shown how they have some chemical properties and whether they comply with these rules. The molecular mass of any molecule did not go above 500 Dalton as well as the first five compounds' biodegradable scores are the same (0.55), others score 0.85. In conclusion, all the molecules adopted in this study fully comply with Lipinski's rules.

Table 6. Data of Lipinski rule, pharmacokinetics, and drug-likeness.

	NBR	HBA	HBD	TPSA	Consensus Log Po/w	Log Kp (skin permeation)	Lipinski rule		MW	Bioavaila-bility Score	GI absorption
							Result	violation			
1	4	3	1	58.22	2.84	-6.04	Yes	0	301.38	0.55	High
2	8	5	0	78.05	4.01	-5.58	Yes	0	376.47	0.55	High
3	8	4	0	56.59	3.25	-6.41	Yes	0	373.49	0.55	High
4	7	5	0	73.34	4.71	-5.63	Yes	0	415.55	0.55	High
5	10	5	1	67.59	3.67	-7.55	Yes	0	469.65	0.55	High
6	8	4	1	68.01	5.22	-4.71	Yes	0	441.56	0.85	High
7	9	4	1	68.0	5.56	-4.41	Yes	0	455.59	0.85	High

2.8 *In silico* pharmacokinetics study by ADMET

The ADMET (absorption, distribution, metabolism, excretion, and toxicity) parameters are essential and vital for post-drug discovery. These parameters provide information as an aid to clinical trials for drug discovery, which can be easily performed by computational chemistry, in a short time, at low cost, and without any accident. Although these drugs have been previously approved for a variety of diseases, their ADMET studies do not carry much information. Yet some of

these parameters are important enough to explain our subject matter with new information and data in our drug discovery. The first thing to be covered is Human Intestinal Absorption (HIA) and its value for all molecules is around 0.9899, which indicates a higher capacity (Table 7). Secondly, they all respond positively to Blood-Brain Barrier (BBB) and are opposite for CYP450 2C9 substrate and CYP450 1A2 inhibitor. Another important point is that all these molecules exist in mitochondria. Finally, ADME has evolved to permit the use of rapid and less expensive methods that have made the early assessment of drug candidates very attractive to the pharmaceutical industry.

Table 7. Data for ADME parameters.

Drug	HIA	Caco-2 Permeability	BBB	P-I glycoprotein inhibitor	P- II glycoprotein substrate	Renal organic cation transporter	Sub-cellular localization	CYP450 2C9 substrate	CYP450 1A2 inhibitor
1	0.9936	0.8198	Yes	Yes	Yes	0.5754	Mitochondria	No	Yes
2	0.9899	- 0.5331	Yes	No	No	0.7914	Mitochondria	No	No
3	0.9940	0.6476	Yes	Yes	Yes	0.6625	Mitochondria	No	No
4	0.9912	-0.6039	Yes	Yes	No	0.6332	Mitochondria	No	No
5	0.9890	-0.6084	Yes	Yes	Yes	0.6184	Mitochondria	No	No
6	0.9863	- 0.5826	Yes	No	Yes	0.6536	Mitochondria	No	No
7	0.9863	-0.6841	Yes	Yes	Yes	0.5823	Mitochondria	No	No

2.9 Aquatic and non-aquatic toxicity

Toxicity assessment for any chemical molecule is one of the most important facts, which play a significant role in formulating their proper use policy. When an object is used in any place, there is a risk of damage to the aquatic and non-aquatic place. This is why it is so important to study their toxicity. For these molecules, we have predicted their toxicity assessment evaluation from the online database. First of all, not all molecules have the potential to cause cancer, and this is true for AMES toxicity. For these compounds, we have done a water solubility assessment with values ranging from -3.571 to -4.008 (Table 8). Therefore, the chances of them polluting the environment are very slim. In addition, Oral Rat Acute Toxicity (LD_{50}) values stay range from 2.2634 to 3.0874 mol/kg.

Table 8. Aquatic and non-aquatic toxicity.

Drug	AMES toxicity	Carcinogenicity	Water solubility, Log S	Plasma protein binding	Acute Oral Toxicity, kg/mol	Oral Rat Acute Toxicity (LD_{50}) (mol/kg)	Fish Toxicity pLC_{50} mg/L	*T. Pyriformis* toxicity (log µg/L)
1	No	No	-3.571	0.700	2.396	3.0874	1.2749	0.4678
2	No	No	-3.578	1.130	2.631	2.2634	1.0219	0.5791
3	No	No	-4.008	0.639	2.275	3.0184	1.0661	0.5895
4	No	No	-3.595	1.148	3.197	2.6050	1.3787	0.4737
5	No	No	-3.630	1.173	2.417	2.7340	1.1890	0.6935
6	No	No	-3.566	0.963	2.829	2.7004	1.6264	0.498
7	No	No	-3.599	0.938	3.142	2.7467	1.4707	0.572

3. Computational Details

3.1 Preparation and optimization of ligand

The seven typical bilastine compounds, acting as anti-allergic drugs, were taken from the PubChem website in SDF form [48]. Material Studio 8.0 was used for geometry optimization [49]. For the optimization, B3LYP of DMol code was used in this software to calculate the chemical reactivity indicators using frequency calculation by density functional theory (DFT) [50]. After optimization, the molecular frontier orbital diagrams of HOMO and LUMO were taken with their magnitude and diagram. The PDB form of molecules was further used for molecular docking as a ligand and was saved as a file.

3.2 Method for molecular docking

The starting three-dimensional (3D) structure of RNA protein of CoV-19 was discovered in December 2019 from Wuhan, China. It was found in Protein Data Bank (PDB) with ID: 5r7y (**https://www.rcsb.org/structure/5r7y**), which was considered as one of the initial strain of CoV-19 virus and established as the RNA strains with all carried genetic characteristics. In addition, the spike protease (6xs6) was taken from PDB with the link: **https://www.rcsb.org/structure/6XS6** [51].

After taking the proteins from PDB, these were viewed by the PyMOL software version using PyMOL V2.3 (**https://pymol.org/2/**) [52]. All water molecules and unexpected ligands or heteroatoms were removed to get fresh protein, and it was saved as PDB files. The PyRx software was used for molecular docking in the term of auto dock vine. After the molecular docking, the docked complexes were taken Discovery Studio version 2017 for result analyses and view [53].

3.3 Determination of the data of ADMET

The ADMET (absorption, distribution, metabolism, excretion, and toxicity) properties were completed by the online database amdetSAR (**http://lmmd.ecust.edu.cn/admetsar2**), which is the most acceptable database for predicting the AMDET parameters [54-56].

3.4 Molecular dynamics (MD)

To perform MD simulations, NAMD software was used to run interactively with live view or in batch mode on a desktop or laptop computer [57, 58]. MD simulation was devoted to supporting the docking results and obtained the best fitting prediction of drugs and CoV-19 protein up to 5000 ns applying AMBER14 force field [59]. In the presence of water as a solvent, the total system was equilibrated with 0.9% NaCl at 298 K temperature. A cubic cell was propagated within 20 Å on every side of the process and periodic boundary circumstances during the simulation. After simulation, the RMSD and RMSF were analyzed using the VMD software.

3.5 Calculation inhibition constant (IC_{50})

The software packet MGLtool 1.5.6 was used in the case of auto dock Vina calculation with adding polar hydrogen and selective active site of the protein. Using these tools, inhibition constant (IC_{50}, μM), ligand efficiency, internal energy (kcal/mol), Vdw-Hydrogen bonding-desolved energy (kcal/mol), electrostatic energy (kcal/mol), torsional energy (kcal/mol), and unbound energy (kcal/mol) were calculated for ligand-protein complex after docking.

4. Conclusions

Important attempts to diagnose computational studies of the derivatives of piperidine-1-carboxylate and sulfonyloxyethyl carboxylate (**1**-**7**) against SARS-CoV-2 M^{pro} and S^{pro} have been successfully conducted. Their chemical reactivity indicators have been shown to be sufficiently active, with the aid of attachment of compounds' HOMO and LUMO with M^{pro} and S^{pro} protein sites. The molecular binding energy of these compounds with these proteins was encouraging and comparable to any standard drugs. Further evidence in favour of this observation was found from ligand-protein complex IC_{50} values. However, superior IC_{50} was found for M^{pro} (12 μM to 70 μM) than S^{pro} (253 μM to 380 μM, except **3** and **5**) indicating better activity against the main protease. Again, in molecular dynamics lower RMSD and RMSF value was found for M^{pro} (0.8 Å) than S^{pro} (1.4 Å). This study significantly indicated that the derivatives of piperidine-1-carboxylate and sulfonyloxyethyl carboxylate (**1**, **3**-**7**) could be able to inhibit M^{pro} and S^{pro} successfully, and comparatively more promising against M^{pro} than that of S^{pro}. The AMDET study, on the other hand, suggested that these compounds are less toxic, can be applied safely without harming the environment.

Supporting Information

Table-S01: Ligand-Protein interaction data for Mpro and Table-S02: Ligand-Protein interaction data for Spro

Acknowledgments

One of us (MM Matin) acknowledges Research and Publication Cell, University of Chittagong for partial financial support to conduct the study.

Author Contributions

All authors equally contributed in design, data collection, analysis, writing, and revision of the manuscript, and MM Matin supervised this project.

References and Notes

[1] Miura, T. A.; Emily, A. T.; Lauren, O.; Helle, B. O.; Susan, R. W.; Nicole, B.; Kathryn, V. H. *J. Virol.* **2008**, *82*, 755. [Crossref]

[2] Mousavizadeh, L.; Sorayya, G. *J. Microbiol. Immunol. Infect.* **2020**, *54*, 159. [Crossref]

[3] De Haan, C. A. M.; Kuo, L.; Masters, P. S.; Vennema, H.; Rottier, P. J. M. *J. Virol.* **1998**, *72*, 6838. [Crossref]

[4] Sarma, P.; Shekhar, N.; Prajapat, M.; Avti, P.; Kaur, H.; Kumar, S.; Singh, S.; Kumar, H.; Prakash, A.; Dhibar, D. P.; Medhi, B. *J. Biomol. Struct. Dyn.* **2020**, *38*, 2724. [Crossref]

[5] Boopathi, S.; Poma, A. B.; Kolandaivel, P. *J. Biomol. Struct. Dyn.* **2021**, *39*, 3409. [Crossref]

[6] Khan, R. J.; Jha, R. K.; Amera, G. M.; Jain, M.; Singh, E.; Pathak, A.; Singh, R. P.; Muthukumaran, J.; Singh, A. *J. Biomol. Struct. Dyn.* **2020**, *39*, 2679. [Crossref]

[7] Khan S. A.; Zia, K.; Ashraf, S.; Uddin, R.; Ul-Haq, Z. *J. Biomol. Struct. Dyn.* **2021**, *39*, 2607. [Crossref]

[8] Gupta, M. K.; Vemula, S.; Donde, R.; Gouda, G.; Behera, L.; Vadde, R. *J. Biomol. Struct. Dyn.* **2021**, *39*, 2617. [Crossref]

[9] Aanouz, I.; Belhassan, A.; El-Khatabi, K.; Lakhlifi, T.; El-Ldrissi, M.; Bouachrine, M. *J. Biomol. Struct. Dyn.* **2021**, *39*, 2971. [Crossref]

[10] Elfiky, A. A.; Azzam, E. B. *J. Biomol. Struct. Dyn.* **2021**, *39*, 2923. [Crossref]

[11] Joshi, R. S.; Jagdale, S. S.; Bansode, S. B.; Shankar, S. S.; Tellis, M. B.; Pandya, V. K.; Chugh, A.; Giri, A. P.; Kulkarni, M. J. *J. Biomol. Struct. Dyn.* **2021**, *39*, 3099. [Crossref]

[12] Enmozhi, S. K.; Raja, K.; Sebastine, I.; Joseph, J. *J. Biomol. Struct. Dyn.* **2021**, *39*, 3092. [Crossref]

[13] Matin, M. M.; Chakraborty, P.; Alam, M. S.; Islam, M. M.; Hanee, U. *Carbohydr. Res.* **2020**, *496*, ID: 108130. [Crossref]

[14] Wahedi, H. M.; Ahmad, S.; Abbasi, S. W. *J. Biomol. Struct. Dyn.* **2021**, *39*, 3225. [Crossref]

[15] Sinha, S. K.; Shakya, A.; Prasad, S. K; Singh, S.; Gurav, N. S.; Prasad, R. S.; Gurav, S. S. *J. Biomol. Struct. Dyn.* **2021**, *39*, 3244. [Crossref]

[16] Abdelli, I.; Hassani, F.; Brikci, B. S.; Ghalem, S. *J. Biomol. Struct. Dyn.* **2021**, *39*, 3263. [Crossref]

[17] Hasan, A.; Paray, B. A.; Hussain, A.; Qadir, F. A.; Attar, F.; Aziz, F. M.; Sharifi, M.; Derakhshankhah, H.; Rasti, B.; Mehrabi, M. *J. Biomol. Struct. Dyn.* **2021**, *39*, 3025. [Crossref]

[18] Gautret, P.; Lagier, J. –C.; Parola, P.; Meddeb, L.; Mailhe, M.; Doudier, B.; Courjon, J.; Giordanengo, V.; Vieira, V. E.; Dupont, H. T. *Int. J. Antimicrob. Agents.* **2020**, *56*, 105949. [Crossref]

[19] Liverton, N. J.; Bednar, R. A.; Bednar, B.; Butcher, J. W.; Claiborne, C. F.; Claremon, D. A.; Cunningham, M.; DiLella, A. G.; Gaul, S. L.; Libby, B. E. *J. Med. Chem.* **2007**, *50*, 807. [Crossref]

[20] Karaman, N.; Sicak, Y.; Taşkın-Tok, T.; Öztürk, M.; Karaküçük-İyidoğan, A.; Dikmen, M.; Koçyiğit-Kaymakçıoğlu, Be.; Oruç-Emre, E. E. *Eur. J. Med. Chem.* **2016**, *124*, 270. [Crossref]

[21] Zhang, L.; Zhan, P.; Chen, X.; Li, Z.; Xie, Z.; Zhao, T.; Liu,

H.; De Clercq, E.; Pannecouque, C.; Balzarini, J. *Bioorg. Med. Chem.* **2014**, *22*, 633. [Crossref]

[22] Kwon, Y. E.; Park, J. Y.; No, K. T.; Shin, J. H.; Lee, S. K.; Eun, J. S.; Yang, J. H.; Shin, T. Y.; Kim, D. K.; Chae, B. S. *Bioorg. Med. Chem.* **2007**, *15*, 6596. [Crossref]

[23] Wang, G.; Chen, L.; Xian, T.; Liang, Y.; Zhang, X.; Yang, Z.; Luo, M. *Org. Biomol. Chem.* **2014**, *12*, 8048. [Crossref]

[24] Fang, Y.; Xu, J.; Li, Z.; Yang, Z.; Xiong, L.; Jin, Y.; wang, Q.; Xie, S.; Zhu, W.; Chang, S. *Bioorg. Med. Chem.* **2018**, *26*, 4080. [Crossref]

[25] Hennequin, L. F.; Stokes, E. S. E.; Thomas, A. P.; Johnstone, C.; Plé, P. A.; Ogilvie, D. J.; Dukes, M.; Wedge, S. R.; Kendrew, J.; Curwen, J. O. *J. Med. Chem.* **2002**, *45*, 1300. [Crossref]

[26] Kuntz, I. D.; Blaney, J. M.; Oatley, S. J.; Langridge, R.; Ferrin, T. E. *J. Mol. Biol.* **1982**, *161*, 269. [Crossref]

[27] Afroza, Z.; Kumer, A.; Sarker, M. N.; Paul, S. *Int. J. Chem. Technol.* **2019**, *3*, 151. [Crossref]

[28] Kumer, A.; Ahmed, M. B.; Arfat, M. S.; Al-Mamun, A. *Asi. J. Phy. Chem. Sci.* **2017**, *4*, 1. [Crossref]

[29] Kumer, A.; Paul, S.; Sarker, M. N.; Mohammad, Islam, J. *Int. J. Chem. Technol.* **2019**, *6*, 236. [Crossref]

[30] Kumer, A.; Sarker, M. N.; Paul, S. *Int. J. Chem. Technol.* **2019**, *3*, 26. [Crossref]

[31] Hoque, M. M.; Kumer, A.; Hussen, M. S.; Khan, M. W. *Int. J. Adv. Biol. Biomed. Res.* **2021**, *9*, 77. [Crossref]

[32] Hoque, M. M.; Hussen, M. S.; Kumer, A.; Khan, M. W. *Mol. Simul.* **2020**, *36*, 1298. [Crossref]

[33] Islam, M. J.; Sarker, M. N.; Kumer, A.; Paul, S. 2019. *Int. J. Adv. Biol. Biomed. Res.* **2019**, *7*, 318. [Crossref]

[34] Matin, M. M.; Ibrahim, M.; Anisa, T. R.; Rahman, M. R. *Malaysian J. Sci.* **2022**, 41(1), 91. [Crossref]

[35] Islam, M. J.; Kumer, A.; Paul, S.; Sarker, M. N. *Chem. Methodologies* **2020**, *4*, 130. [Crossref]

[36] Kumer, A.; Sarker, M. N.; Paul, S. *Int. J. Chem. Technol.* **2019**, *3*, 59. [Crossref]

[37] Kumer, A.; Sarkar, M. N.; Pual, S. *Eurasian J. Environ. Res.* **2019**, *3*, 1. [Crossref]

[38] Kumer, A.; Sarker, M. N.; Paul, S. *Turkish. Comp. Theo. Chem.* **2019**, *3*, 59. [Link]

[39] Babahedari, A. K.; Heidari, S. E.; Shamsabadi, M. K.; Kabiri, H. *J. Bionanosci.* **2013**, *7*, 288. [Crossref]

[40] Hermann, T.; Westhof, E. *J. Med. Chem.* **1999**, *42*, 1250. [Crossref]

[41] Trott, O.; Olson, A. J. *J. Comput. Chem.* **2010**, *31*, 455. [Crossref]

[42] Bertamino, A.; Iraci, N.; Ostacolo, C.; Ambrosino, P.; Musella, S.; Di S. V.; Ciaglia, T.; Pepe, G.; Sala, M.; Soldovieri, M. V. *J. Med. Chem.* **2018**, *61*, 6140. [Crossref]

[43] Liu, K.; Kokubo, H. *J. Chem. Inf. Model.* **2017**, *57*, 2514. [Crossref]

[44] Guterres, H.; Im, W. *J. Chem. Inf. Model.* **2020**, *60*, 2189. [Crossref]

[45] Lipinski, C. A.; Lombardo, F.; Dominy, B. W.; Feeney, P. J. *Adv. Drug Deliv. Rev.* **1997**, *46*, 3. [Crossref]

[46] Daina, A.; Michielin, O.; Vincent, Z. *Sci. Rep.* **2017**, *7*, 42717. [Crossref]

[47] Guex, N.; Peitsch, M. C. *Electrophoresis* **1997**, *18*, 2714. [Crossref]

[48] Kim, S.; Thiessen, P. A.; Bolton, E. E.; Chen, J.; Fu, G.; Gindulyte, A.; Han, L.; He, J.; He, S.; Shoemaker, B. A.; Wang, J.; Yu, B.; Zhang, J.; Bryant, S. H. *Nuc. Acids Res.* **2016**, *44*, D1202. [Crossref]

[49] Ramos, J. **2020**, digital.csic.es. [Link]

[50] Parr R. G.; Yang, W. *J. Am. Chem. Soc.* **1984**, *106*, 4049. [Crossref]

[51] Yurkovetskiy, L.; Wang, Xue,; Pascal, K. E.; Tomkins-Tinch, C.; Nyalile, T. P.; Wang, Y.; Baum, A.; Diehl, W. E.; Dauphin, A.; Carbone, C. *Cell* **2020**, *183*, 739. [Crossref]

[52] DeLano, W. L. **2002**. [Link]

[53] Valentine, D.; Zaslavsky, I.; Richard, S.; Meier, O.; Hudman, G.; Peucker-Ehrenbrink, B.; Stocks, K. *Concurr. Comput.* **2020**, *33*, 01. [Crossref]

[54] Cheng, F.; Li, W.; Zhou, Y.; Shen, J.; Wu, Z.; Liu, G.; Lee, P. W.; Tang, Y. *J. Chem. In.f Model.* **2012**, *52*, 3099. [Crossref]

[55] Matin, M. M.; Bhattacharjee, S. C.; Chakraborty, P.; Alam, M. S. *Carbohydr. Res.* **2019**, *485*, ID: 107812. [Crossref]

[56] Matin, M. M.; Uzzaman, M.; Chowdhury, S. A.; Bhuiyan; M. M. H. *J. Biomol. Struct. Dyn.* **2020**. [Crossref]

[57] Phillips, J. C.; Hardy, D. J.; Maia, J. D. C.; Stone, J. E.; Ribeiro1, J. V.; Bernardi1, R. C.; Buch, R.; Fiorin, G.; Hénin, J.; Jiang, W.; McGreevy, R.; Melo1, M. C. R.; Radak, B. K.; Skeel, R. D.; Singharoy, A.; Wang, Y.; Roux, B.; Aksimentiev, A.; Luthey-Schulten, Z.; Kalé, L. V.; Schulten, K.; Chipot, C.; Tajkhorshid, E. *J. Chem. Phys.* **2020**, *153*, ID: 044130. [Crossref]

[58] Rahman, M. A.; Matin, M. M.; Kumer, A.; Chakma, U.; Rahman, M. R. *Phy. Chem. Res.* **2022**, *10*(2), 189. [Crossref]

[59] Skjevik, A. A.; Madej, B. D.; Dickson, C. J.; Teigen, K.; Walker, R. C.; Gould, I. R. *Chem. Comm.* **2015**, *51*, 4402. [Crossref]

How to cite this article

Kumer, A.; Chakma, U.; Matin, M. M. *Orbital: Electron. J. Chem.* **2022**, *14*, 15. DOI: http://dx.doi.org/10.17807/orbital.v14i1.1642